Hydration heat, strength and microstructure characteristics of UHPC containing blast furnace slag

Yalçinkaya, Çaglar; Çopuroğlu, Oğuzhan

DOI
10.1016/j.jobe.2020.101915

Publication date
2021

Document Version
Final published version

Published in
Journal of Building Engineering

Citation (APA)
Yalçinkaya, Ç., & Çopuroğlu, O. (2021). Hydration heat, strength and microstructure characteristics of UHPC containing blast furnace slag. *Journal of Building Engineering*, *34*, 1-10. Article 101915. https://doi.org/10.1016/j.jobe.2020.101915

Journal of Building Engineering 34 (2021) 101915

Contents lists available at ScienceDirect

Journal of Building Engineering

journal homepage: http://www.elsevier.com/locate/jobe

Hydration heat, strength and microstructure characteristics of UHPC containing blast furnace slag

Çağlar Yalçınkaya [a,b,*], Oğuzhan Çopuroğlu [b]

[a] Dokuz Eylül University, Faculty of Engineering, Department of Civil Engineering, 35160, İzmir, Turkey
[b] Delft University of Technology, Faculty of Civil Engineering and Geosciences, Section Materials & Environment, 2628 CN, Delft, the Netherlands

ARTICLE INFO

Keywords:
UHPC
Blast furnace slag
Hydration heat
Temperature
Microstructure

ABSTRACT

Ultra-high performance concrete (UHPC) is an innovative cement-based composite with high mechanical performance under tensile and compressive loads, extremely low permeability, and excellent durability. Because of these features, UHPC has the potential to contribute to the development of new architectural perspectives and structural systems with prolonged service life; therefore, it is anticipated that the use of UHPC in cast-in-situ applications will increase in the near future. As a result of its high Portland cement dosage, the hydration heat of UHPC can be relatively high compared to that of conventional concrete. Thus, ground granulated blast furnace slag (GGBS) can be used in UHPC formulation for reducing Portland cement dosage thereby limiting hydration heat while also addressing ecological and engineering concerns. In the scope of this study, the effects of GGBS replacement (0%, 30%, and 60%) on the hydration heat, strength, and microstructural characteristics of UHPC were studied. Results showed that GGBS-bearing UHPCs are more sensitive to ambient temperature in respect to cumulative heat. 60% GGBS replacement reduced cumulative heat release by 36% and 28% at 20 °C and 35 °C respectively. So, the benefit of GGBS on reducing hydration heat is less pronounced in hot weather. Performance differences in strength depending on the replacement ratio were only noticeable on the first day of curing. Prolonged curing time and fiber inclusion eliminated strength differences. Microstructural investigations indicated that $Ca(OH)_2$ can be lowered up to 0.5%, and the Ca/Si ratio of the C–S–H phase was reduced below the value of 1.0 after 90 days of curing as a result of GGBS replacement.

1. Introduction

Structural engineers and architects have focused on the use of high-performance concrete in recent decades to ensure that structures are resistant to external influences such as seismic movements and to minimize maintenance costs due to durability problems. Ultra-high performance concrete (UHPC) is a cement-based composite that can exhibit high strength and advanced durability properties as a result of its low water/binder ratio and fine-rich design. Due to its high cement content, the hydration heat of UHPC can be relatively large [1]. As a result, the problems encountered in the production of mass concrete can also be seen in the case of UHPC structural members with reduced cross-sectional areas. Despite the expectation of perfect protection against rebar corrosion from UHPC, thermal or shrinkage-induced cracks can reduce corrosion resistance by disabling the advantages of the dense cementitious matrix that resists the ingress of harmful ions [2–4]. Therefore, researchers have given importance to the use of pozzolanic materials for reducing Portland cement dosage thereby limiting hydration heat and in accordance with both ecological and engineering concerns.

Ground-granulated blast furnace slag (GGBS) is a by-product of the production of pig iron which has been used since the early 1900s as supplementary cementitious material in traditional concrete. Recent studies have shown that GGBS is one of the most suitable supplementary cementitious materials for high performance concretes to reduce cement dosage while enhancing its mechanical properties. Yazıcı et al. [5] reported that the compressive strength of UHPC could be increased by a replacement of up to 40 wt % of cement with GGBS; it was also possible to use of GGBS up to 60% with satisfactory results. Yu et al. [6] studied the development of eco-friendly UHPCs by using efficient mineral admixtures and found that the mechanical properties of UHPC with GGBS were higher than that of UHPCs bearing fly ash or limestone powder. Wu et al. [7] investigated the detailed mechanical performance of UHPC mixtures bearing GGBS or fly ash, and concluded that the optimum

* Corresponding author. Dokuz Eylül University, Faculty of Engineering, Department of Civil Engineering, 35160, İzmir, Turkey.
E-mail addresses: caglar.yalcinkaya@deu.edu.tr (Ç. Yalçınkaya), o.copuroglu@tudelft.nl (O. Çopuroğlu).

https://doi.org/10.1016/j.jobe.2020.101915
Received 14 June 2020; Received in revised form 1 September 2020; Accepted 20 October 2020
Available online 23 October 2020

ratios were 40% and 20% for GGBS and fly ash, respectively. Bae and Pyo [8] emphasized that GGBS can be added to UHPC mixtures to enhance workability as well as to bring down material costs.

The hydration of cementitious materials in UHPC is similar to that in traditional concrete under standard curing conditions. Portland cement hydrates to form calcium silicate hydrate (C–S–H) and $Ca(OH)_2$. Then mineral admixtures such as silica fume, commonly used in UHPC, react with calcium hydroxide to form secondary C–S–H [9]. However, the phase development in UHPC is expected to be kinetically and quantitatively different from that in traditional concretes. In addition, it is expected that heat flux and microstructure will be greatly influenced by incorporating pozzolanic additives [10]. GGBS can produce additional C–S–H upon hydration while decelerating early strength development when there is no activator in the system [11]. However, the hydration rate of the blends with GGBS generally accelerates after five days of hydration because the diffusion of Ca^{2+} and OH^- can be restricted at earlier ages [6]. Hydration is also retarded due to the diluting effect compared with an equivalent increase in the w/c ratio, which suppresses the temperature rise associated with the release of the hydration heat [12].

UHPC is a promising material for reinforced concrete structures because it has significant potential for creating new architectural perspectives as well as structural systems with a prolonged service life and low maintenance costs thanks to its superior durability performance [13]. Due to its hydraulic action, high strength activity, and fineness value [14], GGBS may be one of the best alternative cementitious materials for use in UHPC that will allow for a reduction in Portland cement dosage while maintaining satisfactory performance. It is anticipated that the use of UHPC in cast-in-situ applications will increase in the near future. Since early age hydration heat of UHPC is a central issue for cast-in-situ applications and has a great influence on cracking tendency, it should be studied under different temperature conditions. To date, most strength and microstructure studies of UHPC have been performed up to a standard curing time of 28 days when UHPC cannot reflect its full potential [15]. Thus, in the scope of this study, the effects of the GGBS replacement ratio on the mechanical properties, and microstructure of UHPC after 90 days of moisture-curing were investigated. Moreover, the effects of GGBS replacement on the early age hydration heat release were evaluated at two different temperatures reflecting moderate and hot weather conditions.

2. Experimental

2.1. Materials and mix proportions

GGBS was provided by Orcem BV, the Netherlands. As common cementitious materials of UHPC, Portland cement (CEM I 52.5 R) and silica fume were used. Portland cement was produced by ENCI Company (Heidelberg cement group) in the Netherlands. Densified silica fume was obtained from Elkem Silicon Materials, Norway. The main chemical compositions determined by X-ray fluorescence and selected properties of cementitious materials are given in Table 1. Particle size distributions are shown in Fig. 1. Quartz aggregates were provided by Sibelco, Belgium. The aggregate phase was composed of 40% 0–125 μm and 60% 125–250 μm quartz by mass. High-range water-reducing polycarboxylic ether-based superplasticizer, applicable in UHPC, was used to adjust the slump-flow value of UHPC mixtures. In order to determine the curing time-dependent mechanical properties of fiber-reinforced UHPC mixtures, brass-coated straight micro steel fibers of a length of 13 mm and a diameter of 0.2 mm were incorporated. Micro steel fibers had a reported tensile strength of 2750 MPa and Young's modulus of 200 GPa.

Table 1
Chemical composition and selected properties of cementitious materials.

Chemical Composition (wt %)	Cement	GGBS	Silica Fume
CaO	68.71	42.00	0.42
SiO_2	17.41	30.73	90.38
Al_2O_3	4.62	13.30	0.54
Fe_2O_3	2.75	0.54	3.09
MgO	2.49	9.44	0.67
K_2O	0.63	0.34	1.03
SO_3	2.44	1.45	0.57
Loss on Ignition	1.37	0.57	1.45
Physical Properties			
Strength Activity Index-28d (%)	–	100	125
Fineness (m^2/kg)	530	460	24,250
Specific Gravity	3.15	2.89	2.20

The reference mixture was formulated to exceed a compressive strength level of 150 MPa in presence of micro steel fibers accompanied by self-compacting ability. Silica fume was used at a dosage corresponding to 20% by mass of cement. The water to binder ratio was kept at 0.20. In the second stage, Portland cement was replaced by 30% and 60% GGBS by weight, and three UHPC mixtures were produced in total. Mix proportions are given in Table 2. The superplasticizer dosage was adjusted to reach the target spread value of 310 ± 10 mm. The mini flow cone (60 mm high with diameters of 100 mm at the base and 70 mm at the top) was used for the slump-flow test of self-compacting mixtures. UHPC mixtures were prepared by using a Hobart-type mixer. First, cementitious materials were mixed. Then, the dry ingredients were incorporated into the water + superplasticizer solution. After obtaining fluid paste, quartz aggregates were gradually added to the paste. Finally, high-speed mixing was initiated. The mixing procedure lasted for 18 min for plain UHPCs and 20 min for fiber-reinforced UHPCs (Fig. 2). Reference UHPC without GGBS replacement, UHPC with %30 GGBS replacement, and UHPC with %60 GGBS replacement were denoted as ref., FS30, and FS60, respectively. Mixtures with micro steel fiber reinforcement were coded as ref.-f, FS30-f, and FS60-f. The volume needed for micro steel fiber inclusion was deducted from the volume of the quartz aggregate in the 125–250 μm fractions in order to keep constant water to powder ratio among the mixtures.

2.2. Isothermal calorimetry measurements

To clarify the effect of GGBS replacement and curing temperature on the heat of hydration, the heat flows of the paste phase of UHPCs were monitored by isothermal calorimetry (TAM-Air) over 48 h in accordance with ASTM C1679 [16]. Measurements were taken at temperatures of 20 °C and 35 °C to reflect moderate and hot weather conditions, respectively. All the binders (cement, silica fume, GGBS), mix water, and superplasticizer were prepared and stored at 20 °C during the 24 h before the test. For each mixture, the dry components were mixed with the water + superplasticizer solution for 3 min by using a high-speed mixer, and 6 g of the fresh mixture was put into the glass ampoule. The sample was then moved into the test cell of the calorimeter immediately. A reference vessel filled with fine quartz sand having the same

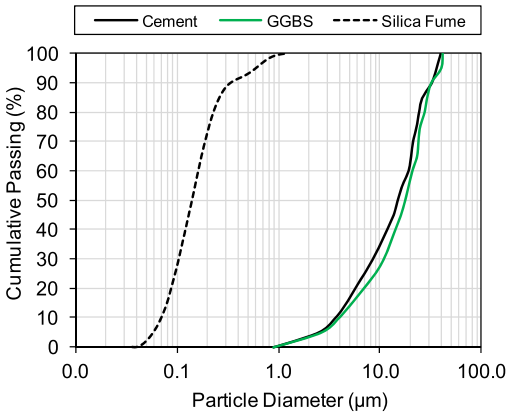

Fig. 1. Particle size distributions of cementitious components.

Table 2
Mix proportions of UHPC mixtures.

Materials (kg/m^3)	Ref.	FS30	FS60	Ref.-f	FS30-f	FS60-f
Water	211	213	215	211	213	215
CEM I 52.5R	881	623	360	881	623	360
GGBS	–	267	540	–	267	540
Silica fume	176	178	180	176	178	180
Quartz (0–125 μm)	372	372	372	372	372	372
Quartz (125–250 μm)	559	559	559	507	507	507
Micro steel-fiber	–	–	–	143.4	143.4	143.4
Superplasticizer	58	44	30	58	44	30
Design Parameters						
GGBS replacement (wt. %)	0	30	60	0	30	60
Water to binder ratio[1]	0.20	0.20	0.20	0.20	0.20	0.20
Paste volume (%)	65	65	65	65	65	65
Micro steel-fiber volume (%)	–	–	–	2	2	2
Slump-flow diameter (mm)	310 ± 10	310 ± 10	310 ± 10	290 ± 10	290 ± 10	290 ± 10

specific heat capacity as the tested paste was also put into a parallel cell. During the test, heat values were recorded at 1-min intervals. Two ampoules for each mixture were tested and there were no observable differences between the results of these two ampoules.

2.3. Mechanical tests

The mechanical properties of UHPC mixtures were evaluated with and without fiber reinforcement. The mechanical properties consisting of compressive and flexural strength were determined after 1, 7, 28, and 90 days of moisture-curing in accordance with the specifications of NEN-EN 196–1 [17]. All the prismatic specimens (40 × 40 × 160 mm^3) were sealed right after casting and kept in a 20 °C environment during the first 24 h. After that, the specimens were demoulded and put into a fog room with a condition of 20°C–100% relative humidity. A three-point bending test was applied to determine the flexural strength. The simply-supported specimens were loaded from their mid-span. A compressive strength test was applied to the two pieces left from the flexural test at a loading rate of 2400 N/s. Six specimens for flexural strength and six specimens for compressive strength were tested for each mixture.

2.4. X-ray diffraction analysis

In order to analyze the mineral phases of UHPC depending on GGBS content, a solid phase analysis was conducted for 90 day-cured UHPC specimens by using X-Ray diffraction (XRD). To obtain suitable powdered samples that were homogenous and fine enough (≤20 μm), hand grinding was applied following a mixer mill. An XRD analysis was performed on the powdered samples using a Philips X'Pert diffractometer applying CuKα radiation (λ = 0.154 nm). The samples were scanned between 5° and 70° 2-theta, with a step size of 0.02° 2-theta and a dwell time of 5 s per step.

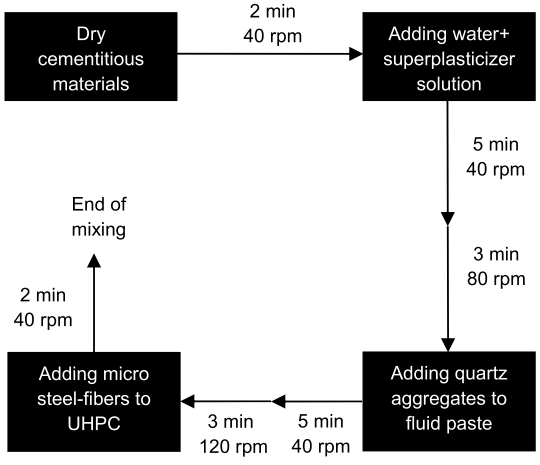

Fig. 2. Mixing procedure of UHPC.

2.5. Thermogravimetric analysis

Thermogravimetric analysis (TGA) was performed to understand the effect of GGBS replacement on the hydration products. Samples were prepared following the same procedure as that of XRD. At 90 days of standard curing, 45 ± 5 mg of the powdered UHPC sample were tested in Argon atmosphere using a Netzsch Sta 449 F3 Jupiter® simultaneous thermogravimetry analyzer. The sample was heated from 40 to 1000 °C at a ramp rate of 20 °C/min.

2.6. Nanoindentation test

Nanoindentation technique involves indenting a surface with a diamond indenter, followed by a loading-unloading cycle while continuously recording the load and indentation depth. From the load-displacement slope and calibrated contact area, the modulus of elasticity of the material can be determined at the micro-scale. An Agilent Nanoindenter G200 (Keysight, Santa Rosa, CA, USA) equipped with a diamond Berkovich tip was used for nanoindentation. Continuous stiffness mode (CSM) was implemented during the nanoindentation test. The CSM was accomplished by imposing a harmonic force, which was added to the nominally increasing load on the indenter. The displacement response of the indenter at the excitation frequency and the phase angle between the two were measured continuously as a function of depth [18]. Measurements were performed after seven days of moisture curing of UHPCs to understand the strength differences observed from a short curing time depending on GGBS replacement. The specimens were cut into slices of 10 mm thickness. They were then ground and polished prior to the test.

2.7. Scanning electron microscopy

The microstructure of specimens was monitored by using a Philips XL30 scanning electron microscope (SEM) at 15 kV accelerating voltage. To carry out the microscopic investigation, 40 × 40 × 160 mm^3 prismatic specimens were produced. For SEM investigations, polished sections were prepared after a 90-day curing period. Prismatic specimens were cut into pieces of 40 × 40 × 10 mm^3 by using a blade saw specially designed for cementitious materials. For backscattered electron (BSE) microscopy, nearly 20 × 20 × 10 mm^3 specimens were ground and polished after epoxy impregnation. Between each of the steps of grinding, an ultrasonic bath was applied for 5 s.

3. Results and discussion

3.1. Hydration heat

Due to high binder content, it was anticipated that UHPC would have a noticeably higher heat of hydration compared to that of traditional concretes. In this study, high replacement ratios of GGBS were implemented to achieve a similar strength level accompanied by a lower heat of hydration than that of conventional UHPC. The heat flow and cumulative heat curves measured at 20 °C and 35 °C for the first 48 h are given in Fig. 3, and Fig. 4, respectively. The given heat values were normalized by the total weight of binders (cement + silica fume + GGBS). The first peak—which was not fully recorded (the test data started to record nearly 30 min after water addition)—was specifically due to the hydration of C_3A which upon dissolution reacts with Ca^{2+} and SO_4^- ions present in the liquid phase to form ettringite (AFt) [19]. At the

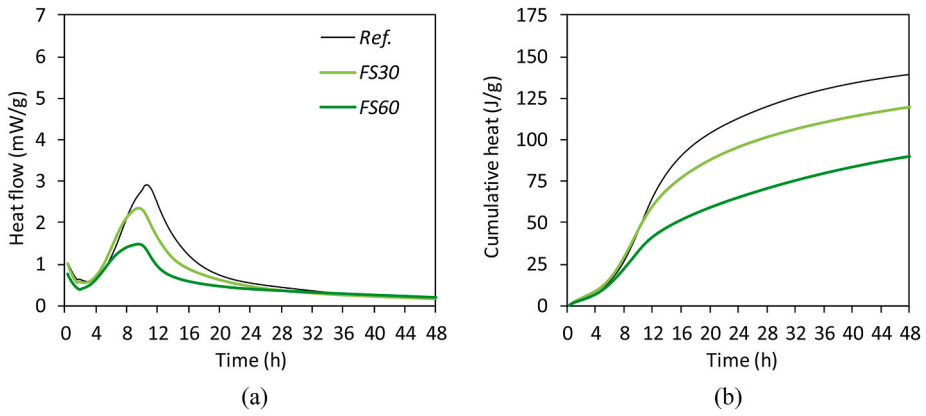

Fig. 3. Heat flow (a) and cumulative heat (b) curves of UHPC pastes at 20 °C.

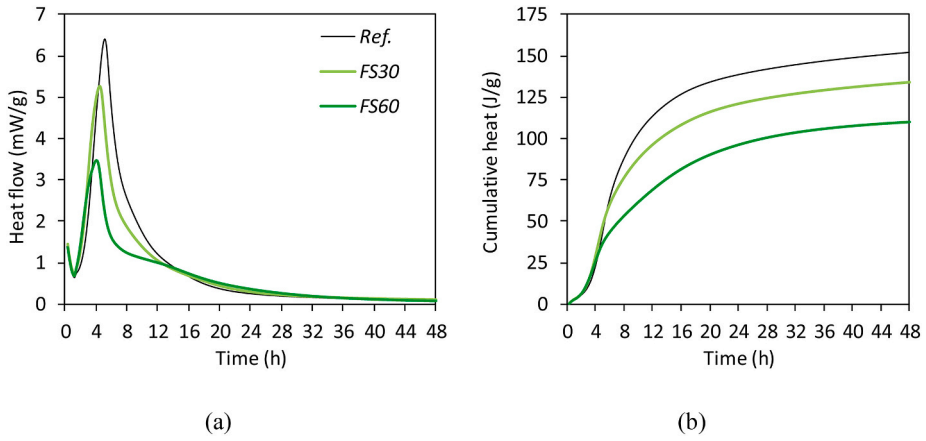

Fig. 4. Heat flow (a) and cumulative heat (b) curves of UHPC pastes at 35 °C.

end of the first peak, there was almost no dormant period as a result of the high amount of silica fume acting as nucleation sites for cement hydration as well as the high early strength effect of the superplasticizer used. This behavior was more prominent at 35 °C than at 20 °C. Then, the main heat flow started to evolve, mainly due to the hydration of C_3S and the initial pozzolanic reactions. GGBS replacement reduced the total heat released and the main peak of the heat flow curve as well. In the case of 20 °C (Fig. 3), the initial rate of heat flow slightly increased during the first 8 h as a result of 30% GGBS replacement. This can be attributed to a reduction in the amount of superplasticizer. The early hydration of binders is usually retarded as a result of high superplasticizer dosage in UHPC [20,21]. GGBS replacement at 60% caused an extensive dilution effect and heat flow started to slow down around 5.5 h as compared to that of the control mixture. When the temperature was 35 °C, a steeper increase in the heat flow rate was observed as a result of GGBS replacement. The increment of the temperature at early age accelerated hydration reactions of the binders and significantly reduced the time needed for achieving peak points of the curves. The peak of heat flow curves at 20 °C was reached at 10.6 h, 9.6 h, and 9.5 h for ref., FS30, and FS60 mixtures, respectively. The peak values at 35 °C were observed at 5.2 h, 4.5 h, and 4 h for ref., FS30, and FS60 mixtures in sequence. The reduction in the time that was needed for achieving the second peak as a result of the temperature increase became slightly more pronounced as GGBS replacement increased. This can be attributed to an accelerated pozzolanic reaction of UHPC due to more $Ca(OH)_2$ formation during the first few hours. FS60 mixture exhibited a shoulder following the main peak at 35 °C, whereas it exhibited a gradual reduction of heat flow at 20 °C. When Portland cement was replaced by GGBS in a high volume (%60), the time needed for the liberation of a sufficient amount of $Ca(OH)_2$ to achieve the correct alkalinity was prolonged [22]. Abdulkareem et al. [23] have observed a similar trend for UHPC mixtures where GGBS content was equal to or higher than Portland cement content, as a result of the dilution effect. Apparently, an increase in the curing temperature made the shoulder formation related to the delayed reaction of GGBS more obvious by accelerating the $Ca(OH)_2$ formation. The cumulative heat releases of ref., FS30, and FS60 mixtures were 140, 120 and 90 J/g at 20 °C, whereas they were 152, 134 and 110 J/g at 35 °C at the end of 48 h, respectively. An increase in the curing temperature increased the total heat release in concordance with the conclusions of the previous studies [24,25]. Moreover, GGBS-bearing mixtures were found to be more sensitive to curing temperature when compared with the control mixture in terms of cumulative heat. 60% GGBS replacement reduced cumulative heat release by 36% and 28% at 20 °C and 35 °C, respectively. As it is seen, the benefits of GGBS on reducing hydration heat are less pronounced in hot weather.

3.2. Strength development

The flexural strengths of UHPC mixtures without and with fiber reinforcement are given in Fig. 5 and Fig. 6, respectively. In the case of plain UHPC without fiber (Fig. 5), GGBS replacement caused a slight decrease in flexural strengths at early age curing. However, when the curing time reached 7 days, flexural strengths for all mixtures were very close and almost the same as that of 28 days. Some previous studies showed that the flexural strength of UHPC could reduce when GGBS replacement surpassed 40% [7,26]. These contradictory findings can be attributed to the difference in mix design parameters and GGBS source used. As a result of the prolonged curing for 90 days, flexural strengths

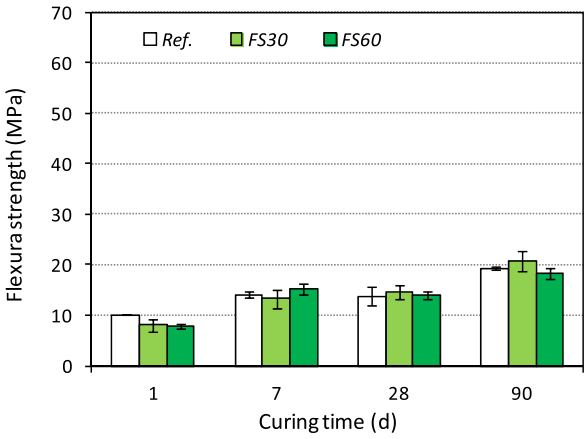

Fig. 5. Flexural strength of UHPC mixtures without fiber.

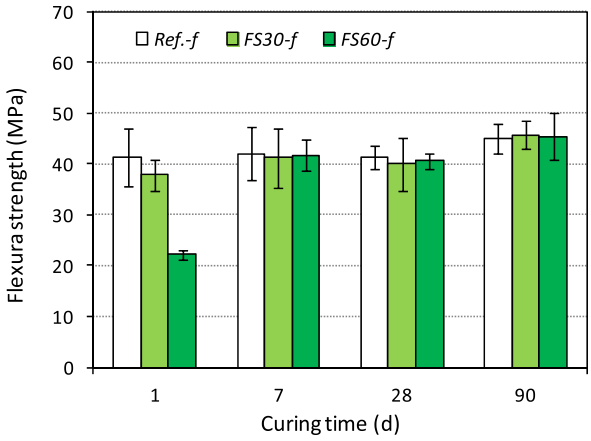

Fig. 6. Flexural strength of fiber-reinforced UHPC mixtures.

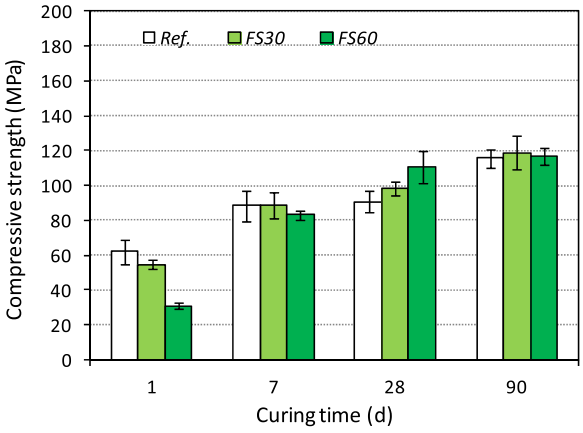

Fig. 7. Compressive strength of UHPC mixtures without fiber.

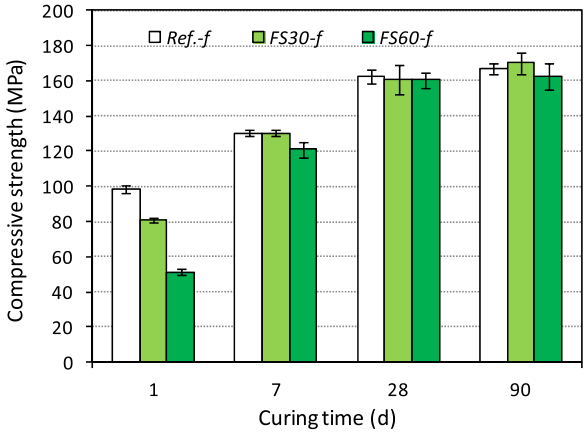

Fig. 8. Compressive strength of fiber-reinforced UHPC mixtures.

were enhanced in the range of 31%–42% compared to 28 days of curing. The increment ratio was found largest for 30% GGBS replacement. When it comes to the fiber-reinforced series (Fig. 6), the FS60 mixture bearing 60% GGBS exhibited an intense curing sensitivity and gained just 54% of the strength of the control mixture at one day. Due to the high volume replacement, the strength differences among the fiber-reinforced UHPCs were greater than those between the plain ones; this indicates that there is an explicit effect of strength development of the matrix on the fiber-matrix bond at an early age. At seven days, flexural strengths exceeded 40 MPa and multiple cracking behaviors were observed for all mixtures. Further increment in flexural strength was observed between 28-day and 90-day curing periods; finally, a very high flexural strength level around 45 MPa was recorded at all GGBS ratios.

Compressive strengths of UHPC mixtures without and with fiber reinforcement are given in Fig. 7 and Fig. 8 respectively. In the case of plain UHPCs without fiber (Fig. 7), 60% GGBS replacement caused a sharp reduction (50%) in compressive strength whereas 30% GGBS replacement caused a 12% strength loss at the end of the first day. At seven days, pozzolanic reactions had taken place and compressive strength in the range of 83–88 MPa was achieved for all mixtures. GGBS-bearing mixtures exceeded the performance exhibited by the control mixture at 28 days. After 90 days of curing, UHPC mixtures exhibited compressive strength in the range of 116–119 MPa. When UHPC was reinforced by micro steel fibers (Fig. 8), an explicit increase in compressive strength in comparison with plain UHPCs was recorded starting from an early age. The compressive strength value of the fiber-reinforced mixtures achieved the level of 120 MPa at seven days. Very similar performances were exhibited by the mixtures at 28-day strength. The prolonged curing period of 90 days did not supply any strength development and an ultimate compressive strength between 163 and 170 MPa was obtained. An equal or better mechanical performance as a result of GGBS replacement of up to 60% was also reported in the previous studies [5,27].

3.3. XRD findings

XRD patterns of UHPC mixtures at the end of the 90-day curing period are given in Fig. 9. The characterizations of hydration products elaborated that the main phases after a long hydration period are Ca$(OH)_2$ and ettringite (AFt). Moreover, there were still peaks of C_3S, C_2S, and C_4AF due to non-hydrated cement particles in cement-rich UHPC mixtures, and these peaks were reduced by GGBS replacement. As a result of GGBS replacement, the Ca$(OH)_2$ peaks reduced and almost disappeared in the case of high-volume replacement (60%). This implies that most of the Ca$(OH)_2$ present in UHPC was consumed by the pozzolanic reactions in concordance with the literature [28,29]. Moreover, some of the peaks related to unreacted cement particles also vanished with an increase in replacement ratio. This can be attributed to the reduced Portland cement content of GGBS-bearing mixtures.

3.4. TGA findings

The thermogravimetry/derivative thermogravimetry (TG-DTG) and differential scanning calorimetry (DSC) curves of UHPCs cured for 90

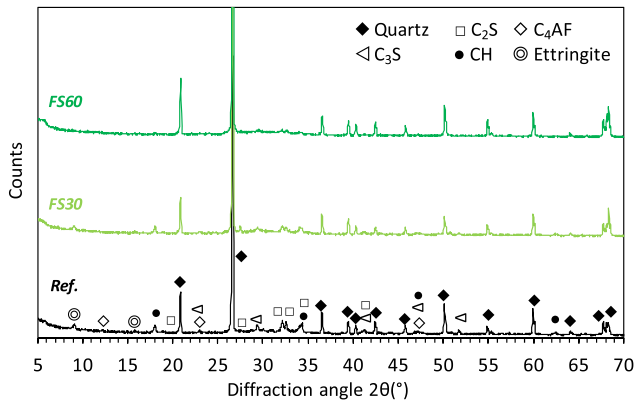

Fig. 9. XRD patterns of UHPC mixtures that were cured for 90 days.

days are given in Fig. 10. The first peak detected under 200 °C is mostly due to the dehydration of several hydrates such as C–S–H, ettringite, monosulfoaluminate, gypsum, and monocarbonate [30]. As a result of GGBS replacement, the main peak located at 139 °C was weakened and shifted to a slightly lower temperature. In the case of 60% GGBS replacement, the peak was located around 127 °C. This can mainly be attributed to a reduction in the amount of unreacted gypsum as well as a reduction in ettringite that was observed in XRD patterns. The second main peak that indicates decomposition of $Ca(OH)_2$ was observed at 471 °C, 468 °C, and 463 °C for Ref., FS30, and FS60 mixtures respectively. The intensity of the peak was weakened by increasing GGBS replacement. In addition to XRD patterns, DTG curves imply that $Ca(OH)_2$ was consumed by the pozzolanic reaction of GGBS. The amounts of $Ca(OH)_2$ were calculated from Fig. 10(a) by implementing a tangential method described in previous studies [31,32]. $Ca(OH)_2$ contents (%) of Ref., FS30, and FS60 were 2.1%, 1.2%, and 0.5%, respectively. Initially, $Ca(OH)_2$ content depends mainly on the fraction of cement content in the matrix, and afterward, it is reduced due to the pozzolanic reaction over curing time [33]. $Ca(OH)_2$ contents decreased with the increasing of GGBS content in concordance with the previous findings [34,35]. At 572 °C, a small endothermic peak was recorded (Fig. 10(b)). Beginning from this temperature, broadband of DTG curve started to form, with a peak at 700 °C. This broad peak can be attributed to the de-carbonation of $CaCO_3$ accompanied by solid-solid transformations [36]. The exothermic peak at 860–875 °C indicates a phase transformation to wollastonite ($CaSiO_3$) [37–39].

3.5. Nanoindentation findings

Nanoindentation test was implemented to measure the moduli of elasticity of the paste phases of UHPC mixtures after the curing period of seven days when the strength values of FS30 and FS60 almost reached that of the reference mixture. Before the test, 25 points from the hydrated phase were selected manually by means of optical microscopy of the nanoindenter. Examples of the curves obtained by nanoindentation are given in Fig. 11(a). The values of Young's modulus were stabilized after the initial indentation depth of 1500 nm due to some effects such as subtraction, surface stress, and roughness [40]. Therefore, elastic moduli were obtained by averaging the corresponding values between 1500 nm and 2000 nm. Elastic moduli of the paste phase of ref., FS30, and FS60 mixtures were found to be 31.2, 32.4, and 27.7 GPa, respectively (Fig. 11(b)). Parallel to the compressive strengths obtained at seven days (Figs. 7 and 8), 60% GGBS replacement notably reduced elastic modulus. Similarly, Hu et al. [41] measured the micromechanical properties of a cement paste with a water to binder ratio of 0.23 by nanoindentation and found that the indentation modulus of C–S–H

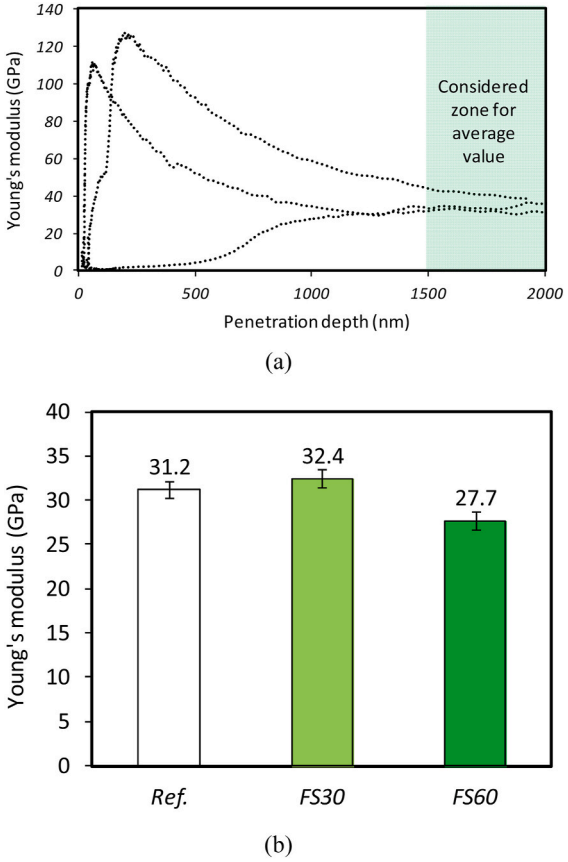

Fig. 11. Typical curves obtained by nanoindentation (a), elastic moduli of paste phases of UHPCs at 7-day (b).

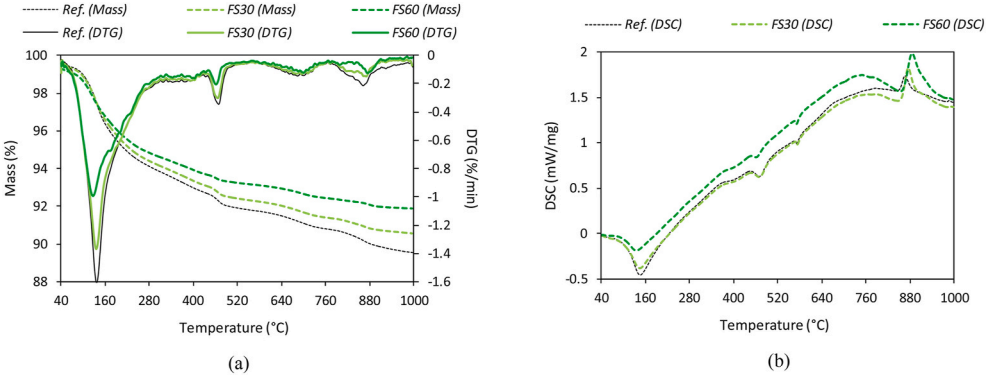

Fig. 10. TG-DTG (a) and DSC (b) curves of UHPC mixtures that were cured for 90 days.

reduced significantly (from 31 to 24 GPa) as a result of 50% GGBS replacement.

3.6. SEM observations

BSE micrographs of ref., FS30, and FS60 mixtures that were cured for 90 days are given in Fig. 12. It was obvious that there was still a large quantity of non-hydrated cement and GGBS particles after the 90-day curing period. Increasing GGBS replacement reduced the cement content, thereby reducing the number of non-hydrated cement particles. However, in this case, unreacted GGBS particles became visible. Moreover, an explicit porosity domain (black area in the images) was noticed even after a long curing period. In the reference mixture, trace amounts of GGBS particles that probably arose from the cement production process were also detected.

During the SEM investigation, a noticeable amount of agglomerates consisting of silica fume particles were detected in the mixtures, particularly in the reference mixture (Fig. 13(a)). Silica fume used in UHPC was in the dry densified form and consisted of agglomerates varying in size from microns to several millimeters. Apparently, the use of densified silica fume in UHPC mixtures with a very low water to cement ratio may result in poor dispersion of the densified particles. GGBS-bearing UHPCs reached the ultimate slump-flow diameter in a shorter time. Even if a viscosity measurement had not been made during the experiments, lower detection of agglomerates in the case of GGBS replacement can be attributed to better dispersion of fines in these mixtures as a result of lower viscosity. In Fig. 13(a), the agglomerate has inner porosity and microcracks. A border that is distinguished as a tight microcrack pattern can be seen around the agglomerate. This particular observation can be attributed to a local volumetric instability that may be associated with an ongoing local alkali-silica reaction which is not harmful to the entire UHPC body [42]. However, when we look deep into the unreacted cement particles, not only the C_2S but also the C_3S phase was observed despite a long curing period. The C_3S phase bearing some impurities on the surface can be differentiated in C_4AF phase in Fig. 13(b). This finding was supported by XRD patterns (Fig. 9). It should be emphasized that although cement with a very high fineness (CEM I 52.5 R) was used, the existence of a considerable amount of unreacted cement particles persisted, even after the 90-day curing period.

In order to compare C–S–H phases of UHPC mixtures, energy dispersive spectrometer (EDS) analyses were performed on five spots that were selected manually during the SEM investigation (Fig. 14). The average Ca/Si ratios were 1.19, 0.92, and 0.88 for ref., FS30, and FS60 mixtures, respectively. In the case of silica-rich cement composite such as UHPC, it is expected that Ca/Si of about 1 can be obtained [43]. The lower Ca/Si demonstrates the overall improved polymerization of C–S–H [44]. By means of silica-rich GGBS replacement, the Ca/Si atomic ratio of C–S–H reduced as a result of the consumption of $Ca(OH)_2$ in the pozzolanic reaction. The determined Ca/Si ratios of moisture-cured mixtures are comparable with that of previous studies [45,46]. The Ca/Si ratio of C–S–H was reported to vary from 1.2 to 2.3 and can reduce with a decrease in the water to binder ratio and the addition of supplementary cementitious materials [47]. Reduction in the Ca/Si ratio enhances the micromechanical properties of the C–S–H phase; however, the results cannot be directly translated into macro mechanical properties of the composite since the compressive strength depends not only on the elastic properties of the C–S–H phase but also on porosity, shrinkage cracks, unreacted particles, presence of aggregates, etc. [48]. Although GGBS replacement reduced the Ca/Si ratio below 1.0, a noticeable increment in the compressive strength of UHPC could not be achieved at 90 days of curing (Fig. 7). A moderate negative linear relationship ($R^2 = 0.62$) between the Ca/Si ratio and the compressive strength of UHPC was reported [43]. Thus, further research is required to confirm a strong relationship between these two properties in the case of very low Ca/Si ratios under the standard curing condition as in this study.

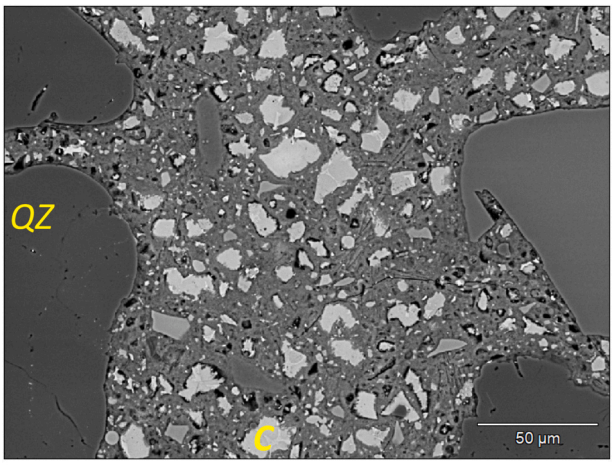

(a)

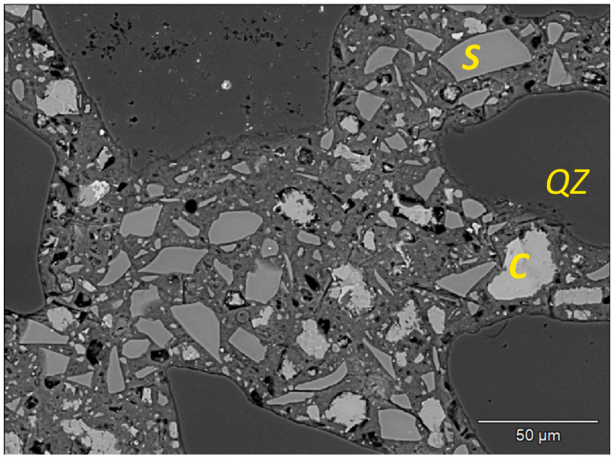

(b)

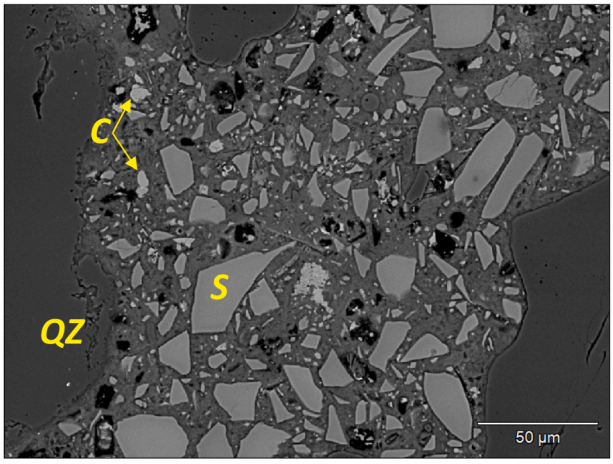

(c)

Fig. 12. BSE micrographs of ref. (a), FS30 (b) and FS60 (b) mixtures that were cured for 90 days (QZ: quartz grain, C: unreacted cement, S: GGBS particle).

4. Conclusions

In this experimental study, calorimetric and microstructural investigations were carried out to clarify the effect of GGBS replacement on the most important engineering properties of UHPCs. The following major conclusions can be drawn:

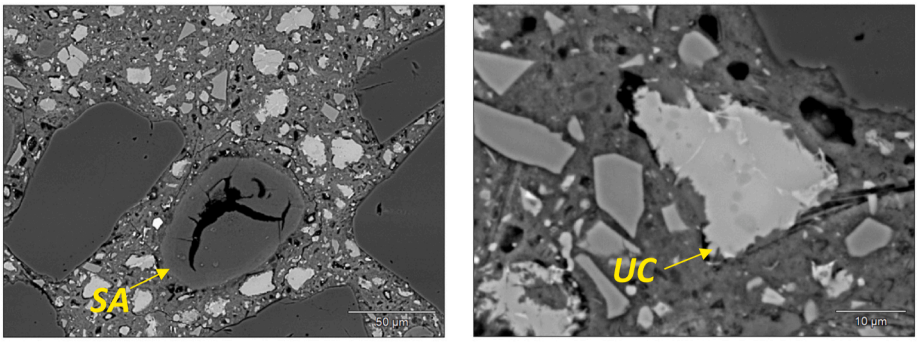

Fig. 13. Typical appearances of silica fume agglomerate (SA) (a), and unreacted cement particle (UC) (b).

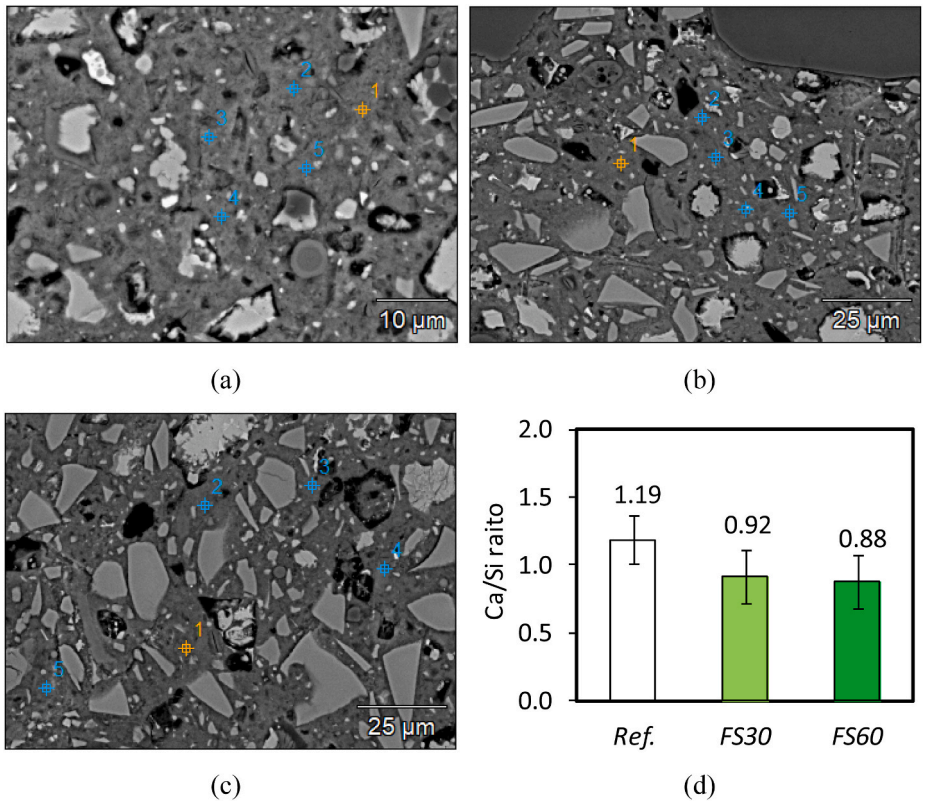

Fig. 14. Spots in ref. (a), FS30 (b), FS60 (c) mixtures that were subjected to EDS analyses, and average Ca/Si ratios (d).

- Replacing Portland cement with GGBS significantly reduced the superplasticizer requirement to reach the target slump-flow value of self-compacting UHPCs. This can ensure a further reduction in the cost of the material in addition to the reduction in cement dosage.
- GGBS replacement reduced both the total heat released and the main peak of the heat flow curve at both 20 °C and 35 °C. An increase in the curing temperature increased the total heat release of UHPC pastes at an early age (48 h). GGBS replaced matrices were found to be more sensitive to curing temperatures when compared with the reference mixture in respect to cumulative heat. 60% GGBS replacement reduced cumulative heat released by 36% and 28% at 20 °C and 35 °C, respectively. In other words, the benefits of GGBS on reducing hydration heat are less pronounced in hot weather. This should be taken into account during hot weather concreting with UHPC.
- As a result of GGBS replacements, strength levels which are nearly the same as those of the reference mixture without GGBS could be achieved. Performance differences in strength values were only noticeable on the first day of the curing period. Prolonged curing time and fiber inclusion eliminated strength differences. Ultimate compressive strength of 160 MPa and flexural strength of 45 MPa were obtained with a cement dosage of only 360 kg/m^3.
- XRD and TGA investigations revealed that as a result of GGBS replacement, main compounds originating from unreacted cement particles as well as $Ca(OH)_2$ content were significantly reduced in the UHPC matrix at the end of the 90-day curing period. $Ca(OH)_2$ could be lowered up to 0.5% in the case of 60% GGBS replacement, indicating that the rest of the $Ca(OH)_2$ amount may not be enough for further pozzolanic reactions despite large numbers of unreacted GGBS particles observed in SEM micrographs.
- Nanoindentation test was carried out to measure the moduli of elasticity of the paste phases of UHPC mixtures after the moisture-curing period of 7 days. High-volume GGBS replacement (60%)

notably reduced the elastic modulus whereas 30% GGBS replacement slightly increased it.
- GGBS replacement reduced the Ca/Si ratio of the C–S–H phase below the value of 1.0 after 90 days of moisture-curing; however, further enhancement in the compressive strength of UHPC could not be observed.

Partial replacement of Portland cement by GGBS reduces the hydration heat while retaining the mechanical performance of UHPC. In this study, a maximum replacement level of 60% which is commonly recommended as the highest percentage for UHPC in the literature was evaluated. However, the effects of the use of slag cement in UHPCs on the engineering properties of UHPCs should be comprehensively investigated to lower the used clinker amount and obtain more eco-friendly mixtures.

CRediT authorship contribution statement

Çağlar Yalçınkaya: Conceptualization, Methodology, Investigation, Visualization, Funding acquisition, Writing - original draft. **Oğuzhan Çopuroğlu:** Supervision, Methodology, Resources, Investigation, Funding acquisition, Writing - review & editing.

Declaration of competing interest

The authors declare that they have no known competing financial interests or personal relationships that could have appeared to influence the work reported in this paper.

Acknowledgments

Çağlar Yalçınkaya would like to acknowledge the postdoctoral research fellowship supported by The Scientific and Technological Research Council of Turkey (TUBITAK). The authors would like to thank Elkem Silicon Materials for material support.

Appendix A. Supplementary data

Supplementary data to this article can be found online at https://doi.org/10.1016/j.jobe.2020.101915.

References

[1] L.A. Sbia, A. Peyvandi, I. Harsini, J. Lu, S.U. Abideen, R.R. Weerasiri, A. M. Balachandra, P. Soroushian, Study on field thermal curing of ultra-high-performance concrete employing heat of hydration, ACI Mater. J. 114 (2017) 733–743, https://doi.org/10.14359/51689677.
[2] E. Erten, Ç. Yalçınkaya, A. Beglarigale, H. Yiğiter, H. Yazıcı, Effect of early age shrinkage cracks on the corrosion of rebar embedded in ultra high performance concrete with and without fibers, J. Fac. Eng Archit. Gaz. 32 (2017) 1347–1364, https://doi.org/10.17341/gazimmfd.369857.
[3] F.U.A. Shaikh, Effect of cracking on corrosion of steel in concrete, Int. J. Concr. Struct. Mater. 12 (2018), https://doi.org/10.1186/s40069-018-0234-y.
[4] L. Hou, B. Zhou, S. Guo, F. Aslani, D. Chen, Corrosion behavior and flexural performance of reinforced concrete/ultrahigh toughness cementitious composite (RC/UHTCC) beams under sustained loading and shrinkage cracking, Construct. Build. Mater. 198 (2019) 278–287, https://doi.org/10.1016/j.conbuildmat.2018.11.237.
[5] H. Yazici, M.Y. Yardimci, H. Yiğiter, S. Aydin, S. Türkel, Mechanical properties of reactive powder concrete containing high volumes of ground granulated blast furnace slag, Cement Concr. Compos. 32 (2010) 639–648, https://doi.org/10.1016/j.cemconcomp.2010.07.005.
[6] R. Yu, P. Spiesz, H.J.H. Brouwers, Development of an eco-friendly Ultra-High Performance Concrete (UHPC) with efficient cement and mineral admixtures uses, Cement Concr. Compos. 55 (2015) 383–394, https://doi.org/10.1016/j.cemconcomp.2014.09.024.
[7] Z. Wu, C. Shi, W. He, Comparative study on flexural properties of ultra-high performance concrete with supplementary cementitious materials under different curing regimes, Construct. Build. Mater. 136 (2017) 307–313, https://doi.org/10.1016/j.conbuildmat.2017.01.052.
[8] Y. Bae, S. Pyo, Ultra high performance concrete (UHPC) sleeper: structural design and performance, Eng. Struct. 210 (2020), https://doi.org/10.1016/j.engstruct.2020.110374.
[9] D. Wang, C. Shi, Z. Wu, J. Xiao, Z. Huang, Z. Fang, A review on ultra high performance concrete: Part II. Hydration, microstructure and properties, Construct. Build. Mater. 96 (2015) 368–377, https://doi.org/10.1016/j.conbuildmat.2015.08.095.
[10] A. Korpa, T. Kowald, R. Trettin, Hydration behaviour, structure and morphology of hydration phases in advanced cement-based systems containing micro and nanoscale pozzolanic additives, Cement Concr. Res. 38 (2008) 955–962, https://doi.org/10.1016/j.cemconres.2008.02.010.
[11] H. Kim, T. Koh, S. Pyo, Enhancing flowability and sustainability of ultra high performance concrete incorporating high replacement levels of industrial slags, Construct. Build. Mater. 123 (2016) 153–160, https://doi.org/10.1016/j.conbuildmat.2016.06.134.
[12] Y.S. Tai, S. El-Tawil, Effect of component materials and mixing protocol on the short-term performance of generic ultra-high-performance concrete, Construct. Build. Mater. 238 (2020), https://doi.org/10.1016/j.conbuildmat.2019.117703.
[13] M. Pezeshkian, A. Delnavaz, M. Delnavaz, Development of UHPC mixtures using natural zeolite and glass sand as replacements of silica fume and quartz sand, Eur. J. Environ. Civ. Eng. (2019), https://doi.org/10.1080/19648189.2019.1610074. In press.
[14] P. Ganesh, A. Ramachandra Murthy, Simulation of surface preparations to predict the bond behaviour between normal strength concrete and ultra-high performance concrete, Construct. Build. Mater. 250 (2020), https://doi.org/10.1016/j.conbuildmat.2020.118871.
[15] H.R. Sobuz, P. Visintin, M.S. Mohamed Ali, M. Singh, M.C. Griffith, A.H. Sheikh, Manufacturing ultra-high performance concrete utilising conventional materials and production methods, Construct. Build. Mater. 111 (2016) 251–261, https://doi.org/10.1016/j.conbuildmat.2016.02.102.
[16] ASTM C1679-14, Standard Practice for Measuring Hydration Kinetics of Hydraulic Cementitious Mixtures Using Isothermal Calorimetry, ASTM International, PA, West Conshohocken, 2014.
[17] NEN-EN 196-1, Methods of Testing Cement - Part 1: Determination of Strength, 2016.
[18] X. Li, B. Bhushan, A review of nanoindentation continuous stiffness measurement technique and its applications, Mater. Char. 48 (2002) 11–36, https://doi.org/10.1016/S1044-5803(02)00192-4.
[19] M. Boháč, M. Palou, R. Novotný, J. Másilko, D. Všianský, T. Staněk, Investigation on early hydration of ternary Portland cement-blast-furnace slag-metakaolin blends, Construct. Build. Mater. 64 (2014) 333–341, https://doi.org/10.1016/j.conbuildmat.2014.04.018.
[20] J. Liu, C. Shi, Z. Wu, Hardening, microstructure, and shrinkage development of UHPC: a review, J. Asian Concr. Fed. 5 (2019) 1–19, https://doi.org/10.18702/acf.2019.12.5.2.1.
[21] S. Sha, M. Wang, C. Shi, Y. Xiao, Influence of the structures of polycarboxylate superplasticizer on its performance in cement-based materials-A review, Construct. Build. Mater. 233 (2020), https://doi.org/10.1016/j.conbuildmat.2019.117257.
[22] E. Gruyaert, N. Robeyst, N. De Belie, Study of the hydration of Portland cement blended with blast-furnace slag by calorimetry and thermogravimetry, J. Therm. Anal. Calorim. 102 (2010) 941–951, https://doi.org/10.1007/s10973-010-0841-6.
[23] O.M. Abdulkareem, A. Ben Fraj, M. Bouasker, A. Khelidj, Mixture design and early age investigations of more sustainable UHPC, Construct. Build. Mater. 163 (2018) 235–246, https://doi.org/10.1016/j.conbuildmat.2017.12.107.
[24] Q. Wang, M. Shi, D. Wang, Contributions of fly ash and ground granulated blast-furnace slag to the early hydration heat of composite binder at different curing temperatures, Adv. Cement Res. 28 (2016) 320–327, https://doi.org/10.1680/jadcr.15.00077.
[25] F. Han, S. Song, J. Liu, R. Wu, Effect of water/binder ratio and temperature on the hydration heat and properties of ternary blended cement containing slag and iron tailing powder, J. Therm. Anal. Calorim. (2020), https://doi.org/10.1007/s10973-020-09687-8. In press.
[26] C.M. Aldea, F. Young, K. Wang, S.P. Shah, Effects of curing conditions on properties of concrete using slag replacement, Cement Concr. Res. 30 (2000) 465–472, https://doi.org/10.1016/S0008-8846(00)00200-3.
[27] P. Ganesh, A.R. Murthy, Tensile behaviour and durability aspects of sustainable ultra-high performance concrete incorporated with GGBS as cementitious material, Construct. Build. Mater. 197 (2019) 667–680, https://doi.org/10.1016/j.conbuildmat.2018.11.240.
[28] L. Yujing, Z. Wenhua, W. Fan, W. Peipei, Z. Weizhao, Y. Fenghao, Static mechanical properties and mechanism of C200 ultra-high performance concrete (UHPC) containing coarse aggregates, Sci. Eng. Compos. Mater. 27 (2020) 186–195, https://doi.org/10.1515/secm-2020-0018.
[29] J. Seo, S. Park, H.N. Yoon, H.K. Lee, Effect of CaO incorporation on the microstructure and autogenous shrinkage of ternary blend Portland cement-slag-silica fume, Construct. Build. Mater. 249 (2020), https://doi.org/10.1016/j.conbuildmat.2020.118691.
[30] W. Wongkeo, P. Thongsanitgarn, P. Chindaprasirt, A. Chaipanich, Thermogravimetry of ternary cement blends: effect of different curing methods, J. Therm. Anal. Calorim. 113 (2013) 1079–1090, https://doi.org/10.1007/s10973-013-3017-3.
[31] F.T. Isfahani, E. Redaelli, F. Lollini, W. Li, L. Bertolini, Effects of nanosilica on compressive strength and durability properties of concrete with different water to binder ratios, Adv. Mater. Sci. Eng. 2016 (2016) 1–16, https://doi.org/10.1155/2016/8453567, 8453567.
[32] Y.A. Villagrán-Zaccardi, H. Egüez-Alava, K. De Buysser, E. Gruyaert, N. De Belie, Calibrated quantitative thermogravimetric analysis for the determination of portlandite and calcite content in hydrated cementitious systems, Mater. Struct. 50 (2017) 179, https://doi.org/10.1617/s11527-017-1046-2.

[33] C. Shi, D. Wang, L. Wu, Z. Wu, The hydration and microstructure of ultra high-strength concrete with cement-silica fume-slag binder, Cement Concr. Compos. 61 (2015) 44–52, https://doi.org/10.1016/j.cemconcomp.2015.04.013.
[34] K. Sisomphon, L. Franke, Evaluation of calcium hydroxide contents in pozzolanic cement pastes by a chemical extraction method, Construct. Build. Mater. 25 (2011) 190–194, https://doi.org/10.1016/j.conbuildmat.2010.06.039.
[35] J. Liu, R. Guo, The microstructures of hardened composite binders containing steel slag and GGBS at 10 years, Construct. Build. Mater. 225 (2019) 1152–1159, https://doi.org/10.1016/j.conbuildmat.2019.08.026.
[36] W. Sha, Differential scanning calorimetry study of the hydration products in portland cement pastes with metakaolin replacement, in: Adv. Build. Technol., Elsevier, 2002, pp. 881–888, https://doi.org/10.1016/B978-008044100-9/50111-X.
[37] J. Chang, Y. Fang, Quantitative analysis of accelerated carbonation products of the synthetic calcium silicate hydrate(C-S-H) by QXRD and TG/MS, J. Therm. Anal. Calorim. 119 (2015) 57–62, https://doi.org/10.1007/s10973-014-4093-8.
[38] H. seok So, H. seok Jang, J. Khulgadai, S. young So, Mechanical properties and microstructure of reactive powder concrete using ternary pozzolanic materials at elevated temperature, KSCE J. Civ. Eng. 19 (2015) 1050–1057, https://doi.org/10.1007/s12205-015-0015-y.
[39] K. Pimraksa, S. Hanjitsuwan, P. Chindaprasirt, Synthesis of belite cement from lignite fly ash, Ceram. Int. 35 (2009) 2415–2425, https://doi.org/10.1016/j.ceramint.2009.02.006.
[40] X. Long, X. Zhang, W. Tang, S. Wang, Y. Feng, C. Chang, Calibration of a constitutive model from tension and nanoindentation for lead-free solder, Micromachines 9 (2018), https://doi.org/10.3390/mi9110608.
[41] C. Hu, Z. Li, Y. Gao, Y. Han, Y. Zhang, Investigation on microstructures of cementitious composites incorporating slag, Adv. Cement Res. 26 (2014) 222–232, https://doi.org/10.1680/adcr.13.00029.
[42] S. Diamond, S. Sahu, N. Thaulow, Reaction products of densified silica fume agglomerates in concrete, Cement Concr. Res. 34 (2004) 1625–1632, https://doi.org/10.1016/j.cemconres.2004.01.031.
[43] S.H. Ghasemzadeh Mosavinejad, M.A.M. Langaroudi, J. Barandoust, A. Ghanizadeh, Electrical and microstructural analysis of UHPC containing short PVA fibers, Construct. Build. Mater. 235 (2020), https://doi.org/10.1016/j.conbuildmat.2019.117448.
[44] H. Zhang, T. Ji, B. He, L. He, Performance of ultra-high performance concrete (UHPC) with cement partially replaced by ground granite powder (GGP) under different curing conditions, Construct. Build. Mater. 213 (2019) 469–482, https://doi.org/10.1016/j.conbuildmat.2019.04.058.
[45] K. Liu, R. Yu, Z. Shui, X. Li, X. Ling, W. He, S. Yi, S. Wu, Effects of pumice-based porous material on hydration characteristics and persistent shrinkage of Ultra-High Performance Concrete (UHPC), Materials 12 (2018), https://doi.org/10.3390/ma12010011.
[46] H. Yazici, E. Deniz, B. Baradan, The effect of autoclave pressure, temperature and duration time on mechanical properties of reactive powder concrete, Construct. Build. Mater. 42 (2013) 53–63, https://doi.org/10.1016/j.conbuildmat.2013.01.003.
[47] I.G. Richardson, Nature of C-S-H in hardened cements, Cement Concr. Res. 29 (1999) 1131–1147, https://doi.org/10.1016/S0008-8846(99)00168-4.
[48] W. Kunther, S. Ferreiro, J. Skibsted, Influence of the Ca/Si ratio on the compressive strength of cementitious calcium-silicate-hydrate binders, J. Mater. Chem. A. 5 (2017) 17401–17412, https://doi.org/10.1039/c7ta06104h.